Sustainable Energy, Grids and Networks 36 (2023) 101152

Contents lists available at ScienceDirect

Sustainable Energy, Grids and Networks

journal homepage: www.elsevier.com/locate/segan

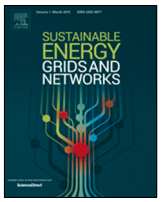

Development, validation, and testing of advanced mathematical models for the optimization of BESS operation

Filippo Bovera [a,*], Matteo Spiller [a], Matteo Zatti [b], Giuliano Rancilio [a], Marco Merlo [a]

[a] Department of Energy, Politecnico di Milano, Via Lambruschini 4, 20156 Milano, Italy
[b] Laboratorio Energia e Ambiente Piacenza (LEAP), Via Nino Bixio 27/c, 29121 Piacenza, Italy

ARTICLE INFO

Article history:
Received 7 April 2023
Received in revised form 15 July 2023
Accepted 16 August 2023
Available online 22 August 2023

Keywords:
Performance modeling of BESS
Mathematical formulation of performance
Operational optimization of BESS

ABSTRACT

Current decarbonization strategies are driven by the fast-paced diffusion of non-programmable renewable energy sources (NP-RESs), mainly through solar and wind power generation. Energy storage technologies are emerging as key solutions for coping with the variability and low-inertia characteristics of NP-RESs. Particularly, battery energy storage systems (BESS) are diffusing more widely for both behind-the-meter (BTM) and utility-scale applications. In this context, we still lack a shared solution on how to proceed from the on-field data collected about the performance of BESS to reliable and fast mathematical formulations for operational optimization. This study provides a validated modeling framework that can be exploited during or after BESS commissioning to (i) identify and derive the useful parameters to characterize BESS performances, (ii) formalize them in a mathematical formulation while being aware of its specific trade-off between accuracy and computational effort, and (iii) exploit the selected BESS model within a multi-energy system optimization problem. We discuss three different modeling approaches that we developed for optimizing BESS operation, with each providing a different balance between modeling accuracy and computational effort. These three mathematical models were validated against a numerical simulation model based on on-field performance data, and they were eventually tested on a reference case study. The results indicate that it is possible to restrict the average error in estimating BESS efficiency while simultaneously limiting the computational effort of the model. Regarding the operation of BESS, the conducted simulations demonstrate that an approximate BESS model may result in an overestimation of the expected revenues.

1. Introduction

Current decarbonization schemes are mainly driven by the proliferation of renewable energy sources (RES), especially wind and photovoltaic (PVs) [1]. Owing to the high variability and intermittency in production using RESs, the security and reliability of networks that transmit electricity is being threatened [2]. Particularly, it is well-known that inverter-based power generation decreases the inertia in power systems, thereby increasing both the number and magnitude of frequency fluctuations [3]. Moreover, the unpredictability of non-programmable power resources results in the need for repeatedly using flexibility services offered by system operators; these include a very short activation time and high power gradients [4]. This condition is exacerbated by the gradual decommissioning of conventional generators, reducing the generation of baseload power and raising the need for time-shift energy consumption or production [5,6].

In this scenario, storage systems are supposed to play a fundamental role in (i) coping with frequency instability and production uncertainty and (ii) meeting energy demands through generation. Particularly, battery energy storage systems (BESS) are among the most promising storage technologies because of their high efficiency and fast response times; furthermore, they have recently surged in industrial development and their production costs have significantly reduced [7,8]. According to the International Energy Agency (IEA), annual global storage additions have increased from below 1 GW in 2015 to above 5 GW in 2020, with lithium-ion technologies currently playing a leading role. The IEA also forecasts a worldwide BESS storage potential of almost 600 GW by 2030, with a substantial balance between behind-the-meter (BTM) and utility-scale applications [9].

Despite decreasing cost projections, investors are still struggling to understand how to maximize the revenues generated by storage investments. The possibility of revenue stacking is a solution often studied in existing literature [10–12]. This consists of exploiting the same BESS for multiple purposes, such as energy arbitrage, peak shaving, or flexibility provision. Thus, the elaboration of a procedure based on complex analysis to carefully assess

* Corresponding author.
E-mail address: filippo.bovera@polimi.it (F. Bovera).

https://doi.org/10.1016/j.segan.2023.101152

and govern BESS operations is becoming increasingly relevant for investors. On the other hand, researchers are trying to understand how it is possible to properly model BESS performance, providing accurate evaluations. This usually implies a trade-off between maintaining the detail in the models and increasing the computational effort.

Research has typically focused on the performance simulation of BESS, with an emphasis on increasing the efficiency of the electrochemical processes taking place within the cells [13–16] and battery management system (BMS) emulation, which involves carefully handling the energy conversion and transformation occurring outside battery cells [17,18]. Instead, the present study targets the whole energy transformation chain in BESS, including aspects such as electrochemical cell efficiency, power conversion system (PCS) performance, and BMS dynamics, all within a single modeling approach. Additionally, BESS auxiliary systems have been treated separately with an ad-hoc representation.

Considering this approach, this study also proposes, validates, and tests three different mathematical formulations for the advanced modeling of BESS operations, allowing the inclusion of BESS performance evaluation within operational optimization problems. Modeling the complexity mainly addresses the possibility, within the presented formulations, of handling how BESS performance is influenced by current operating conditions, including the state of charge (SoC), requested power level, and external ambient conditions. Model testing and validation have been carried out with a focus on the trade-off between accuracy and computational effort; a range of specific comparative parameters has been assessed. Computations have been carried out, in all cases, using a commercial out-of-the-shelf solver (Gurobi).

The paper contribute is twofold. First, the study validates a modeling framework that can be exploited during or after the commissioning of a BESS to characterize and simulate its operational performance. Based on the developed mathematical formulations, an operator:

- gains knowledge of the parameters suitable to characterize BESS performance in a sufficient way,
- owns a set of validated modeling approaches to simulate BESS operations with a well-known accuracy and computational efficiency, and
- can use the selected modeling framework within a more complex optimization problem, encompassing different services provided by the BESS, including arbitrage, peak shaving and frequency regulation.

Second, three mathematical formulations are introduced and discussed, each offering a different trade-off between accuracy and computational effort. This enables the asset manager to make an informed choice based on current boundary conditions, primarily including the optimization horizon, power delivery time, number of controlled assets, and services provided.

The remainder of this paper is organized as follows. Section 2 presents a review of the most important approaches for the numerical modeling of BESS performance. Section 3 introduces three models that provide different mathematical approaches to appropriately include the consideration of BESS performance in optimization problems. Section 4 describes the validation of the developed models in terms of accuracy and computational effort using the IEC 62660-1 standard. Section 5 tests the presented mixed-integer linear programming (MILP)-based models used to measure the impact of different modeling accuracies on the financial aspects of a case study where BESS provides BTM services. Finally, Section 6 presents the main conclusions and plans for future work.

2. Review of literature approaches and numerical models for BESS performance simulation

The accuracy of BESS performance models plays a fundamental role in correctly estimating the possible revenues coming from both BTM and front-of-the-meter (FoM) applications, especially when multiple services are being stacked. In existing literature, three main approaches can be found: electrochemical, equivalent circuit, and empirical models.

Electrochemical models try to directly represent the physical phenomena taking place in battery cells, thus accurately emulating both the dynamics of the electrochemical reactions and the equilibrium conditions reached at the end of these reactions. This approach grants a high accuracy at the cost of a huge computational effort [19].

The equivalent circuit models provide a compromise between the accuracy and computational effort, modeling a battery as an electric circuit featuring a voltage source (or a capacitor) and a series of impedances (usually R-C circuits) to emulate specific phenomena [20,21]. These models have been exploited for a wide range of applications, including online controllers implemented on a BMS [22].

Finally, empirical models exploit the mathematical correlations between the operating variables of BESS to emulate electric and electrochemical phenomena and thereby reproduce BESS performance [23]. The variables usually considered include the alternating current (AC) and direct current (DC) and the SoC of the storage. BESS performance is determined through experimental campaigns or on-field data [24], and then, variables are correlated in specific equations to reproduce BESS behavior. Although this approach reduces the computational effort, it often results in limited accuracy [24]. The number of errors increases when real-life operating conditions are far from experimental ones; on the other hand, tests covering all the performance maps are expensive and invasive; thus, they can hardly be performed on deployed systems [23]. Table 1 provides an overview of the most frequently used and important empirical models found in existing literature, highlighting the presence of two main approaches: MILP and the meta-heuristic (MH) approach. MILP has been considered the more reliable solution for the optimization of complex district energy systems [25]; advantageously, it can uniquely identify the global optimum with a shorter computational time than the MH algorithms can.

Optimizing the BESS performance for quasi-real-time operations requires a high modeling accuracy. Regarding this, the constant efficiency model widely adopted in existing literature lacks an understanding of the non-linearities of BESS performance. Moreover, further elements, including auxiliary power consumption and BMS limits, which have a fundamental role in BESS operation, need to be considered [37]. On top of that, it is difficult to understand how to properly derive a performance map for BESS operations, especially including information about its capability curve and auxiliaries consumption.

Sakti et al. in [38] derive a non-linear formulation of internal losses for an electrochemical cell and scale it up to simulate the performances of a 10 MW BESS. The utilized approach is based on a detailed modeling of phenomena linked to cell thermodynamics, charge conductivity, charge transfer and mass transport, through a set of specific equations. Hence, model characterization is based on laboratory tests conducted on a single cell (Sanyo 2.05 Ah Li-NMC), then scaling up the obtained parameters to simulate a utility scale BESS. Thus, authors model BESS losses as a function of the exchanged power and of the state-of-charge, highlighting an over-estimation up to 10% of arbitrage-related revenues by a constant efficiency BESS model when compared to an enhanced representation.

Table 1
Main approaches found in existing literature for modeling BESS.

Reference	Modeling technique	Modeling of BESS performance			
		Electrochemical efficiency	Auxiliary consumption	Capability limits for BMS	Inverter performance
[26]	Evolutionary algorithm	Constant	NO	NO	YES
[27]	Decomposition method - dynamic programming	Constant	NO	NO	YES
[28]	Decomposition method - dynamic programming	Constant	NO	NO	NO
[29]	Mixed-integer linear programming	Constant	NO	NO	NO
[30]	Decomposition methods - dynamic programming	Constant	NO	NO	NO
[31]	Swarm intelligence- based technique	Constant	NO	NO	NO
[32]	Mixed-integer linear programming	Constant	NO	NO	YES
[33]	Mixed-integer linear programming	Constant	NO	NO	NO
[34]	Evolutionary algorithm	Constant	NO	NO	NO
[35]	Mixed-integer linear programming	Constant	NO	NO	YES
[36]	Evolutionary algorithm	Constant	NO	YES	NO

A different approach is presented by Park et al. in [39]. In this case, battery losses are expressed as a function of the internal cell resistance, resulting in a non-linear function correlating the charging efficiency with the charging power. In addition, inverter efficiency is considered constant. Authors compare a stair-wise formulation, approximating the 1-D non-linear BESS efficiency function, with a conventional average efficiency model. The exploitation of the two approaches for peak shaving and energy arbitrage applications shows that a dynamic simulation of BESS efficiency improves the accuracy of obtained results, even if it entails a major computational effort.

Pandzic et al. in [40] propose a laboratory procedure to obtain the dependence between the battery charging capability and its state of charge. They use experimental results to accurately represent BESS efficiency considering the reduced charging capacity after battery's switching from constant-current to constant-voltage charging, which is especially significant for high C-rate charging. The effect of constant-voltage charging is linearized through a piecewise curve correlating the state-of-charge variation capability (hence the charging power) with the state-of-charge of the battery. Authors test the developed model against a constant charging power limit approach, obtaining that the latter results to be over-conservative, and that the proposed representation is able to fulfill and overcome the day-ahead schedule, in particular if the BESS is working at low C-rate values (0.2C is tested).

While it is complex to accurately model BESS non-linearities, the literature review highlights also the importance of moving from a proper estimation of BESS performances. Three main approaches can be derived from above cited works. First, electrochemical or electrical models emulate the behavior of cells, including chemical, physical and thermodynamic phenomena. However, on one hand this approach implies very complex equations that are hard to be linearized, on the other hand it typically excludes a set of elements that heavily influence BESS performances but are not directly related to cell's behavior, such as power conversion systems and auxiliaries. Second, performance maps often used for empirical models are derived from laboratory tests. Also in this case, the main drawback is related to the difference between on-bench efficiency and on-field performances; the latter can differ due to specific contingencies linked to the ambient conditions and to some possible differences in cells' manufacturing. Third, system wide approaches focus on testing the real-life performances of the overall BESS architecture, including cells, conversion systems and auxiliaries. The advantage is to obtain on-field results that are expected to be more accurate than laboratory tests. The main limitation consists in the difficulty of covering all the performance maps with expensive and invasive on-field tests, and in the current lack of experience about BESS aging effects on real-life applications. This work aims at providing a modeling framework where it is possible to parametrize BESS efficiency starting from an empirical BESS performance map derived from on field testing. The analysis moves form the results presented by Rancilio et al. in [23]; a similar approach is proposed in [41] although, in this second case, the correlation between efficiency and state of charge is not adequately evaluated.

Rancilio et al. in [23] presented an empirical model including three main elements, as reported in Fig. 1. The first element includes battery cells and the power conversion system (PCS), comprising DC-AC conversion (inverter) and voltage transformation (transformer). The second element consists of the BMS, which controls the operation of the battery in real-time through the so-called capability curve. The third element includes all the auxiliaries, such as heating, ventilation, and air conditioning (HVAC); alarms; supervisory and data acquisition (SCADA); and monitoring systems. This three-element-based architecture was used as a reference for the analysis carried out in this study.

The BESS performance has been simulated through a 3-D performance map where the BESS efficiency depends on the SoC and AC side power needed from the BESS, including losses in the electrochemical reactions within the battery pack and PCS [23]. The efficiency surface results from the linear interpolation of points sampled during a campaign experiment. These sampling points are represented as white dots in Fig. 2(a), and their linear interpolation represents the BESS performance map. The output efficiency obtained from the BESS performance map can be used for calculating the requested DC-side power and the consequent variation in SoC (i.e., the variation in the BESS energy content). The BMS is responsible for maintaining the safety of BESS operations, limiting the output power for some specific SoC conditions. Particularly, as shown in Fig. 2(b), the discharging power is limited for SoC values that are too low, and the charging power is limited when the SoC of the BESS is close to 100%; such constraints result from the maximum and minimum voltage thresholds managed by the BMS. The application of power limits imposed by the capability curves allows the final DC-side power and actual corresponding SoC variation to be calculated.

3. Mathematical formulations for modeling of BESS performance

MILP involves discrete and non-discrete decision variables with linear objective functions and constraints. It is widely used in optimization problems for planning and scheduling applications owing to its relatively simple resolution owing to the availability of very efficient commercial solvers and the guarantees for global optimality.

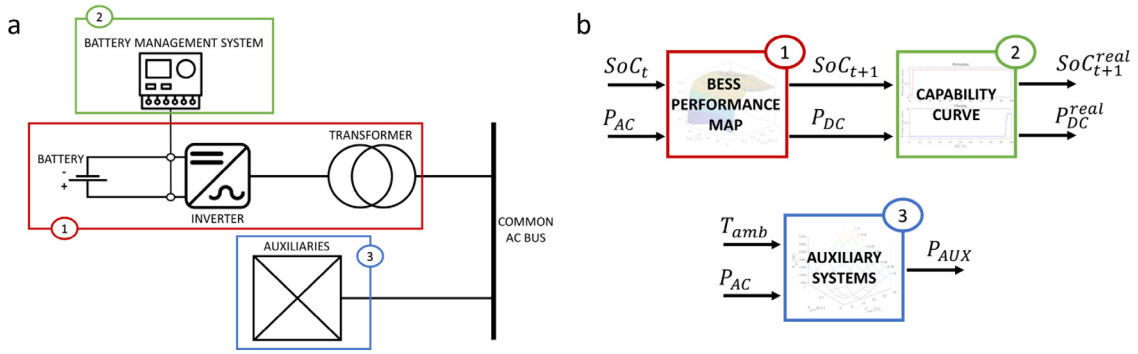

Fig. 1. (a) Operational and (b) modeling architectures for BESS system representation.

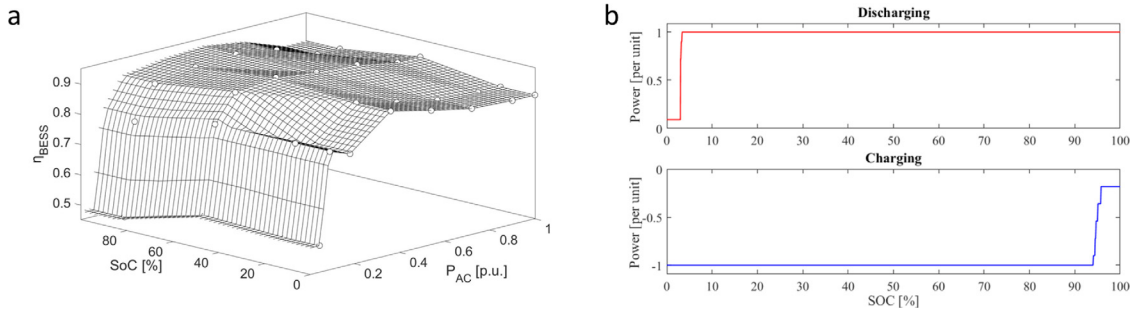

Fig. 2. (a) BESS performance map for evaluation of storage efficiency. (b) BESS capability curves that represent BMS limits.

As presented in Section 2, BESS modeling is characterized by several nonlinearities, including BESS efficiency, capability limits, and auxiliary consumption. In this section, we introduce three different MILP-based mathematical approaches to deal with the non-linearities of BESS efficiency; these models implement a piecewise linearization of the BESS performance map with diverse strategies. Each approach has advantages and drawbacks, mainly in terms of the modeling accuracy and computational effort. The objective is to develop a library of possible formulations to accurately model the BESS performance within the optimization problems typically used for the daily scheduling of energy storage assets. Moreover, the presented models could use any performance data coming from either on-field experimental campaigns or ad-hoc simulations as inputs, showing potential for accurately representing the real-life behavior of a BESS through a detailed mathematical model.

The following sub-sections describe these three formulations, introducing the most important characteristic constraints for each. The mathematical formulation for each modeling approach is completely described in Appendix A. The overall modeling approach is complemented by two further sets of constraints that deal with the BMS capability limits and the energy consumption of the auxiliary systems. The corresponding mathematical formulation is presented in Appendix B.

3.1. First approach: triangle formulation

The first MILP-based formulation builds on the linearization of the BESS performance map through an ensemble of flat triangles; accordingly, it is called triangle formulation. The sampling points representing the BESS performance map were elaborated to develop two look-up tables (LUTs), characterizing either the discharging or charging phase. The obtained LUTs correlated the SoC and DC-side and AC-side powers, and they are made of 3-tuples:

Table 2
BESS performance look-up table (LUT) for triangle formulation of discharging phase.

P_{AC} [p.u.]		SoC [%]				
		0	15	50	85	100
P_{DC} [p.u.]	0	**0.0000**	**0.0000**	**0.0000**	**0.0000**	**0.0000**
	0.05	**0.0367**	**0.0367**	**0.0371**	**0.0346**	**0.0346**
	0.09	**0.0826**	**0.0826**	**0.0826**	**0.0798**	**0.0798**
	0.18	**0.1628**	**0.1628**	**0.1737**	**0.1704**	**0.1704**
	0.36	**0.3464**	**0.3464**	**0.3503**	**0.3447**	**0.3447**
	0.54	**0.5109**	**0.5109**	**0.5210**	**0.5199**	**0.5199**
	0.72	**0.6708**	**0.6708**	**0.6914**	**0.6861**	**0.6861**
	0.9	**0.8351**	**0.8351**	**0.8519**	**0.8341**	**0.8341**
	1.07	**1.0012**	**1.0012**	**1.0213**	**1.0000**	**1.0000**

- $[P_i^{dis,DC}, SOC_j^{dis}, P_{i,j}^{dis,AC}]$ for the LUT for the discharging phase
- $[P_i^{cha,AC}, SOC_j^{cha}, P_{i,j}^{cha,DC}]$ for the LUT for the charging phase.

Table 2 presents the LUT elaborated for the discharging phase: it correlates the SoC and DC-side power with the AC-side power. Considering the roundtrip efficiency reported in [23], assuming the same efficiencies for the charging and discharging phases, the LUT for the charging phase can be defined in a similar way.

Given that four adjacent sampling points belong to the LUT, it is possible to isolate the rectangle resulting from the union of these points and draw two triangles cutting it along the diagonal. The obtained triangles can be distinguished as upper and lower triangles that share a hypotenuse; this is presented in Fig. 3(a), where the 2-D representation of four adjacent rectangles pivoting around a sampling point (i,j) is shown. Fig. 3(b) expands a single rectangle to a 3-D representation, where two flat triangles approximate the curved surface representing a slice of the BESS performance map. Finally, the full piecewise linearization for the LUT of the discharging phase used in the triangle formulation takes the form shown in Fig. 3(c). A corresponding linearization was also performed for the LUT of the charging phase.

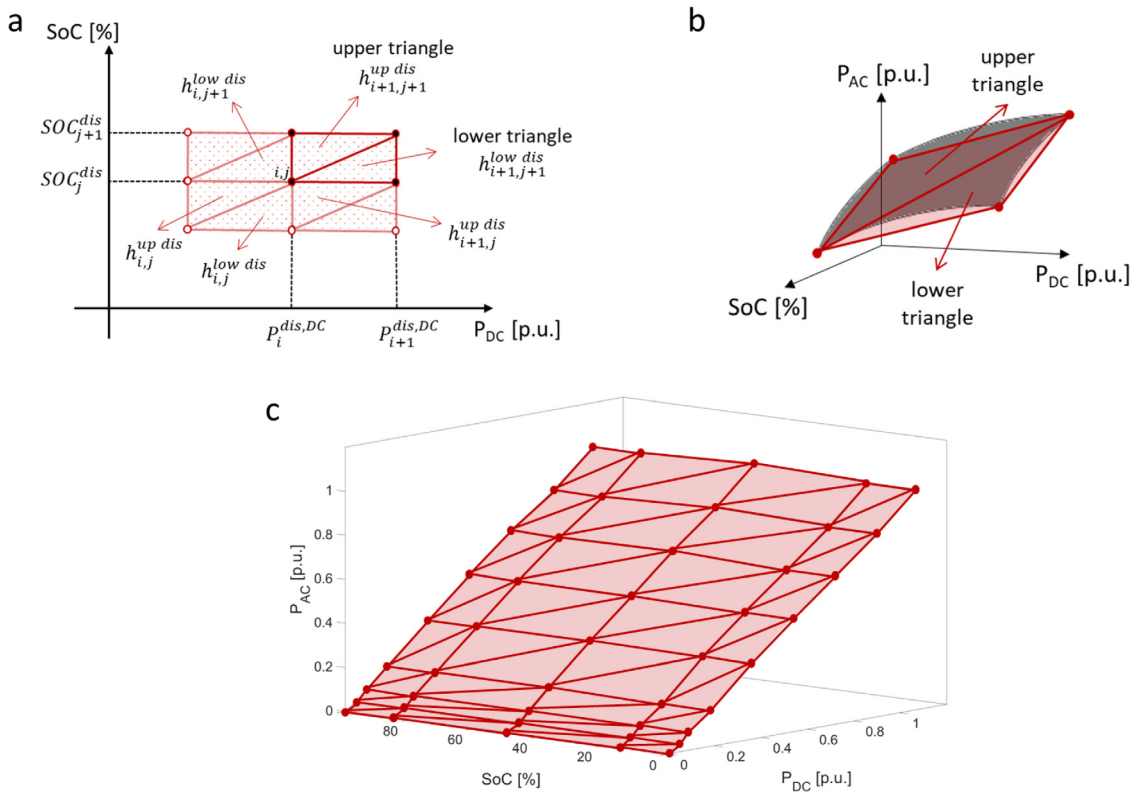

Fig. 3. (a) 2-D graphical representation of triangle formulation approach. (b) 3-D graphical representation of triangle formulation approach. (c) Application of triangle formulation approach to 3-D BESS performance map.

The current AC-side power provided by the BESS was calculated by selecting a single triangle h among all the triangles constituting the linearized BESS performance map, as shown in Fig. 3(c). The selected triangle was uniquely defined by three vertices, corresponding to three sampling points (e.g., $[i,j]\,[i+1,j]\,[i+1,j+1]$). The final values of the AC-side power and those of the corresponding SoC and DC-side power were obtained by properly weighting these three sampling points, moving within the flat area that defined the selected triangle.

The described procedure is expressed through the following mathematical constraints:

$$\sum_i \sum_j y^{cha}_{i,j,t} = z^{cha}_t,\ 0 \le y^{cha}_{j,t} \le 1 \qquad \forall t \qquad (1a)$$

$$\sum_i \sum_j y^{dis}_{i,j,t} = z^{dis}_t,\ 0 \le y^{dis}_{j,t} \le 1 \qquad \forall t \qquad (1b)$$

$$z^{cha}_t + z^{dis}_t \le 1 \qquad \forall t \qquad (1c)$$

$$\sum_i \sum_j \left(h^{up\ cha}_{i,j,t} + h^{low\ cha}_{i,j,t}\right) = z^{cha}_t \qquad \forall t \qquad (1d)$$

$$\sum_i \sum_j \left(h^{up\ dis}_{i,j,t} + h^{low\ dis}_{i,j,t}\right) = z^{dis}_t \qquad \forall t \qquad (1e)$$

$$h^{up\ cha}_{i+1,j+1,t} + h^{low\ cha}_{i+1,j+1,t} + h^{low\ cha}_{i,j+1,t} + h^{up\ cha}_{i+1,j,t} + h^{up\ cha}_{i,j,t} + h^{low\ cha}_{i,j,t} \ge y^{cha}_{i,j,t} \qquad \forall t \qquad (1f)$$

$$h^{up\ dis}_{i+1,j+1,t} + h^{low\ dis}_{i+1,j+1,t} + h^{low\ dis}_{i,j+1,t} + h^{up\ dis}_{i+1,j,t} + h^{up\ dis}_{i,j,t} + h^{low\ dis}_{i,j,t} \ge y^{dis}_{i,j,t} \qquad \forall t \qquad (1g)$$

where t identifies the time; $y^{dis}_{i,j,t}$ and $y^{cha}_{i,j,t}$ are continuous variables ranging from 0 to 1 used to assign a weight to each sampling point; $\left(h^{up\ cha}_{i,j,t}, h^{low\ cha}_{i,j,t}\right)$ and $\left(h^{up\ dis}_{i,j,t}, h^{low\ dis}_{i,j,t}\right)$ are binary variables used to select the corresponding triangle; and z^{cha}_t and z^{dis}_t are binary variables regulating the charging/discharging dichotomy. The full set of constraints used for the triangle formulation is reported and illustrated in Appendix A.

The dense interpolation of the performance map under the triangle method is expected to accurately represent BESS efficiency; however, owing to the large number of variables, especially binary variables, a high computational effort will be needed to solve the optimal scheduling problem. To solve this issue, we developed a mathematical formulation that could model BESS efficiency through a simplified representation of the performance map.

3.2. Second approach: stepwise formulation

The second MILP-based formulation involves approximating the BESS performance map through a stepwise function where the efficiency value in the contour of a sampling point $[i,j]$ is kept constant and equal to the sampling point value. This makes it possible to linearize the BESS efficiency in a stepwise manner; however, this will result in the limitation of step-way variation between a working operation point and the adjacent ones.

Stepwise LUTs are developed through the parametrization of three quantities linked to BESS operations: power required, SoC, and BESS operating efficiency. Fig. 4(a) presents the stepwise formulation concept in a 2-D graphical form. The efficiency profile at a fixed SoC value (corresponding to index j) and for different P_{AC} levels is indicated by a black line. A step function (in red) is built around each sampling point such that the efficiency is considered constant within a specific interval i in the contour of a sampling point. Fig. 4(b) represents the 3-D evolution of the stepwise concept: the red contour of each sampling point (where efficiency is constant) is now a 2-D space, enabling the construction of many stepwise, flat surfaces for different values of both SoC and P_{AC}.

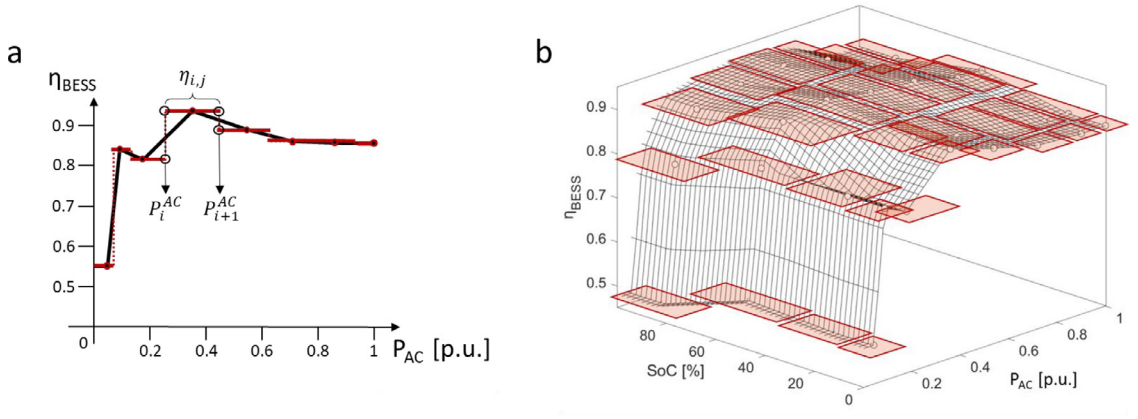

Fig. 4. (a) 2-D graphical exemplification of stepwise approach; and (b) approximation of BESS performance map through stepwise formulation.

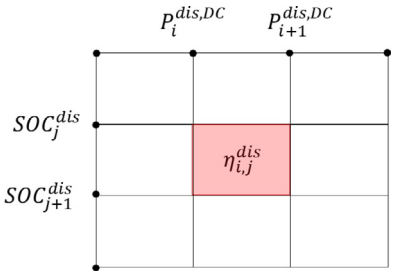

Fig. 5. Graphical representation of a single cell of the LUT for the discharging phase.

In the stepwise formulation, each LUT (both charge and discharge phases) appears as a 2-D array, wherein every single efficiency value corresponds to a cell delimited by two subsequent breakpoints of power (along i) and SoC (along j), as shown in Fig. 5. This means that:

- for the discharging phase, $\eta_{i,j}^{dis}$ is identified by $\left(P_i^{dis,DC}, P_{i+1}^{dis,DC}\right)$ and $\left(SOC_j^{dis}, SOC_{j+1}^{dis}\right)$; and
- for the charging phase, $\eta_{i,j}^{cha}$ is identified by $\left(P_i^{cha,AC}, P_{i+1}^{cha,AC}\right)$ and $\left(SOC_j^{cha}, SOC_{j+1}^{cha}\right)$.

The breakpoints for power and SoC lie halfway between the sampling points of the performance map (see Fig. 2(a)). This means that the number of breakpoints in the stepwise LUTs will be respectively $(I+1)$ and $(J+1)$, where I and J are the number of sampled points in Fig. 2(a).

Through the mathematical formulation of the stepwise approach, a cell from the LUTs for the charging and discharging phases that models the current BESS operations can be chosen. The following constraints are used for this selection: $x_{i,j,t}^{cha}$ and $x_{i,j,t}^{dis}$, which are binary variables used to activate a specific cell (i.e., a power-SoC interval $[i, j]$) in a given time instant t; and z_t^{cha} and z_t^{dis}, which are binary variables that regulate the charging/discharging dichotomy. The full set of constraints used for the stepwise formulation is reported and illustrated in Appendix A.

$$\sum_i \sum_j x_{i,j,t}^{dis} = z_t^{dis}, x_{i,j,t}^{dis} \in [0,1] \qquad \forall t \qquad (2a)$$

$$\sum_i \sum_j x_{i,j,t}^{cha} = z_t^{cha}, x_{i,j,t}^{cha} \in [0,1] \qquad \forall t \qquad (2b)$$

$$z_t^{dis} + z_t^{cha} \leq 1 \qquad \forall t \qquad (2c)$$

$$x_{i,j,t}^{cha} * P_{i,t}^{cha,AC} \leq p_{i,j,t}^{cha,AC} \leq x_{i,j,t}^{cha} * P_{i+1,t}^{cha,AC} \qquad \forall t \qquad (2d)$$

$$x_{i,j,t} * P_{i,t}^{dis,DC} \leq p_{i,j,t}^{dis,DC} \leq x_{i,j,t} * P_{i+1,t}^{dis,DC} \qquad \forall t \qquad (2e)$$

$$x_{i,j,t}^{cha} * SOC_{j,t}^{cha} \leq soc_{i,j,t}^{cha} \leq x_{i,j,t}^{cha} * SOC_{j+1,t}^{cha} \qquad \forall t \qquad (2f)$$

$$x_{i,j,t}^{dis} * SOC_{j,t}^{dis} \leq soc_{i,j,t}^{dis} \leq x_{i,j,t} * SOC_{j+1,t}^{dis} \qquad \forall t \qquad (2g)$$

The stepwise formulation, which includes a few binary variables, is expected to reduce the computational effort required with respect to that under the triangle approach. In the stepwise formulation, the accuracy of the modeling and the computational effort increase with the number of steps considered; consequently, a proper trade-off is required.

3.3. Third approach: fast-piecewise formulation

The two formulations proposed thus far have contrasting characteristics. The triangle formulation is more accurate in emulating the BESS performance but requires more variables and constraints. On the other hand, the stepwise formulation exploits a few variables and requires lower computational effort but at the cost of a reduced accuracy. Considering this, the third approach attempts to reduce the number of variables needed with respect to the triangle model while keeping the accuracy of the model as high as possible. This limits the computational time, making the approach fast enough to be applicable in situations where almost real-time BESS operations are needed. Accordingly, this formulation is called fast-piecewise formulation.

In fast-piecewise formulation, the operating setpoint of the BESS is determined by assigning a weight to each sampling point without imposing that the interpolating points be adjacent. This means that it is possible to avoid introducing the triangle variables h, providing freedom for choosing how to appropriately weight each sampling point of the LUTs in the optimization procedure. The LUTs were again defined in terms of AC-side power, DC-side power, and SoC.

However, the absence of these "proximity" constraints risks hindering the modeling accuracy because of two main issues. First, if the LUT is highly nonlinear, the interpolation between two nonconsecutive sampling points is very detrimental. This is clearly represented for the generic 2-D case in Fig. 6(a), where a non-linear function is presented; this shows how interpolation between two distant sampling points induces a large modeling error. To solve this problem, it is necessary to split the curve (and thus the LUT) into more parts, which reduces the error but increases the formulation complexity (Fig. 6(b)). This linearity problem is not an issue for representing the BESS performance because the surface in Fig. 3(a) shows limited nonlinearity.

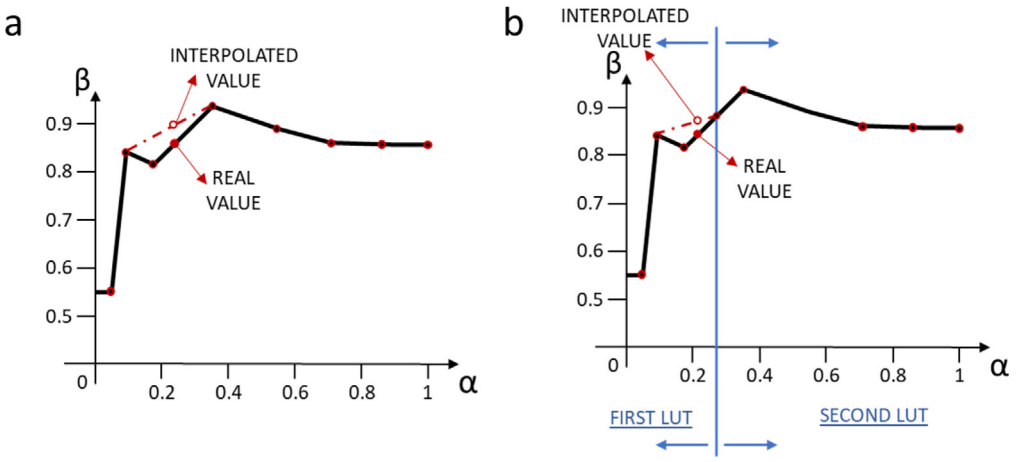

Fig. 6. (a) Interpolation error due to the absence of the proximity constraint in fast-piecewise formulation; (b) solution for the modeling error induced by the absence of the proximity constraint that is obtained splitting the curve, and consequently the corresponding LUT, in two parts.

Second, because fast-piecewise LUTs are not ordered (i.e., the concept of adjacency does not exist), it is not possible to include a zero-power sampling point among them. Indeed, this would introduce strong nonlinearity because the efficiency is not defined for a power setpoint equal to zero (i.e., $\eta_{BESS} = \frac{P_{AC}^{dis}}{P_{DC}^{dis}} = \frac{0}{0} = ND$); this is demonstrated using the numerical example in Appendix C.

Due to this second issue, the formulations of fast-piecewise LUTs do not include zero-power values. To provide the possibility of idle BESS operations during optimization (i.e., power set-point equal to zero), a further binary variable that identifies moments in the idle condition, has been introduced (z_t^{idle}). Overall, the fast-piecewise formulation is based on

- two 3-D LUTs for the discharging ($[P_j^{dis,DC}, SOC_j^{dis}, P_j^{dis,AC}]$) and charging ($[P_i^{cha,AC}, SOC_i^{cha}, P_i^{cha,DC}]$) phases, equivalent to the one exploited under triangle formulation, with the exclusion of zero-power points; and
- one 1-D LUT for the idle condition (SOC_k^{idle}), including only SoC values (AC-side and DC-side powers are equal to zero (by definition) and can hence be neglected).

The absence of the proximity constraint in the fast-piecewise formulation allows for a more slender formulation, as reported below, where $y_{j,t}^{dis}$, $y_{i,t}^{cha}$ and $y_{k,t}^{idle}$ are continuous variables ranging from 0 to 1 that were used to perform the linear interpolation between the sampling points of the LUT in a given time instant t. The summation over the points within the LUT should be either 1 or 0, depending on whether the BESS is charging, discharging, or idle; accordingly, z_t^{cha}, z_t^{dis} and z_t^{idle} are binary variables regulating the charging, discharging, or idle trichotomy operations.

$$\sum_j y_{j,t}^{dis} = z_t^{dis}, \quad 0 \le y_{j,t}^{dis} \le 1 \quad \forall t \tag{3a}$$

$$\sum_i y_{i,t}^{cha} = z_t^{cha}, \quad 0 \le y_{j,t}^{cha} \le 1 \quad \forall t \tag{3b}$$

$$\sum_k y_{k,t}^{idle} = z_t^{idle}, \quad 0 \le y_{k,t}^{idle} \le 1 \quad \forall t \tag{3c}$$

4. Model validation: measurement of performances of developed MILP-based formulations

The MILP-based formulations were compared to the numerical simulation presented in [23] for comparison; a common power set-point was placed on a generic BESS whose performances were alternatively modeled through the three MILP-based formulations and the numerical model presented in [20]. Tests were conducted on a 32 GB RAM and Intel I9X-8 core 4 GHz processor.

Fig. 7 shows the power profile adopted in the validation procedure, which was obtained from the IEC 62660-1 testing profile. The exploited power profile ranged from 1 p.u. in the discharge mode to 0.5 p.u. in the charging mode and lasts for 400 min. Modifications with respect to the IEC 62660-1 cycle were introduced to cover the entire BESS capacity, which ranged from 100 to 0% SoC during testing. The BESS characteristics considered for the validation procedure coincided with a nominal energy of 1000 kWh and a nominal power of 440 kW for an Energy-to-Power Ratio (EPR) of 2.27.

Three key performance indicators (KPIs) were exploited for the validation procedure:

- Mean Average Error (MAE) of BESS efficiency (Eq. (4a));
- MAE of SoC profile (Eq. (4b)); and
- Maximum SoC error evaluated with respect to the overall energy cycle (Eq. (4c)).

The third indicator, called the SoC Maximum Relative Error (MRE), is calculated as the maximum SoC differential between the numerical simulation and MILP-based models (expressed in kWh), divided by the total energy cycled by the BESS during testing.

$$MAE_{efficiency} = \frac{1}{n}\sum_{i=1}^{n} efficiency_{simulink,i} - efficiency_{pyomo,i} \tag{4a}$$

$$MAE_{SOC} = \frac{1}{n}\sum_{i=1}^{n} SoC_{simulink,i} - SoC_{pyomo,i} \tag{4b}$$

$$MRE_{SoC} = \frac{\Delta SoC_{max} * E_{nom}}{\int P_{AC}^{BESS} \cdot dt} \tag{4c}$$

4.1. Results of validation procedure

The results of the validation procedure are reported in Fig. 8. As already mentioned, the numerical simulation presented in [23] was used as a reference benchmark. The comparison results revealed that the triangle formulation showed the highest accuracy in estimating the BESS efficiency, both in terms of shape and absolute terms. The fast-piecewise formulation performed well when the BESS was operated at standard SoC values, but showed some errors when the BESS was discharging at very low SoC values. Finally, the stepwise model was less accurate, with differences in both the shape and the efficiency value, which varied between +4 and −2%.

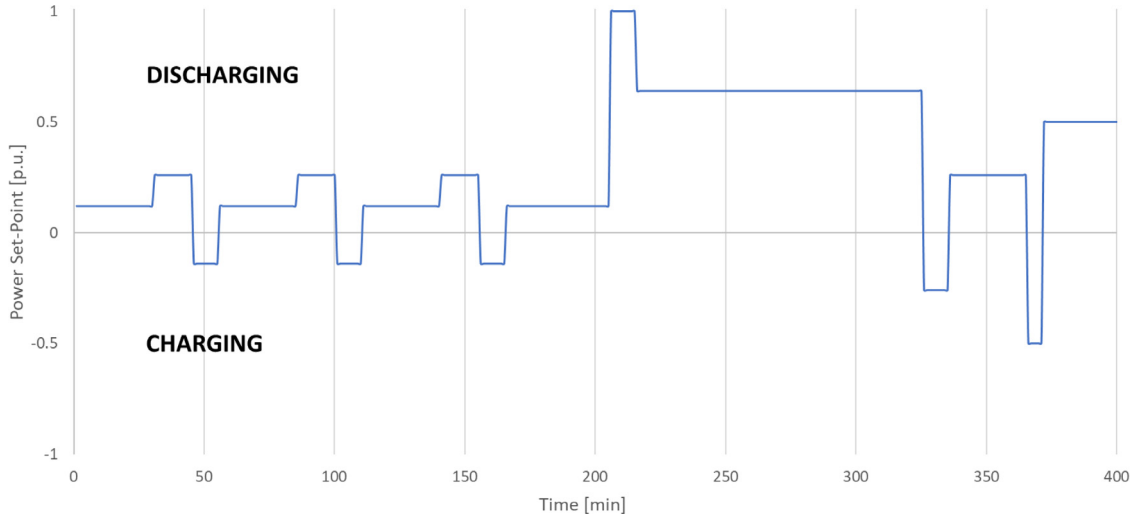

Fig. 7. Test cycle adopted for the validation procedure of the three MILP-based formulations.

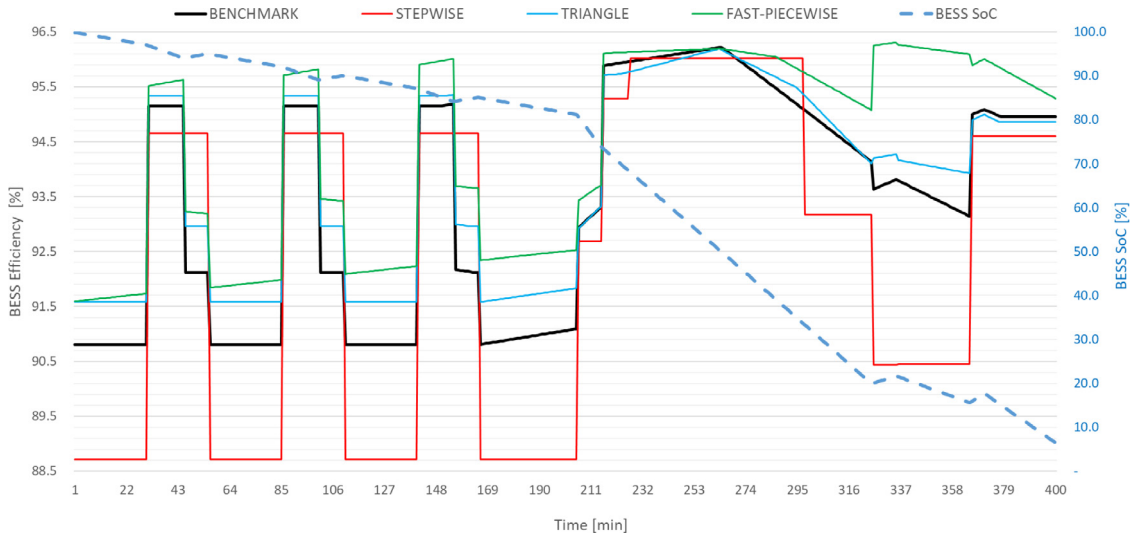

Fig. 8. Comparison of BESS efficiency evaluated on the validation cycle with that of the developed MILP-based formulations and the benchmark numerical simulation presented in [20].

Regarding the efficiency, the estimation of the SoC profile could also be used as a proxy for modeling the accuracy. Fig. 9 shows that the SoC profiles are substantially aligned; however, differences sprung up as time passed due to the differences in the charging/discharging efficiencies and the intervention of capability limits when the SoC value became low. This suggested that the real and estimated (using the model) values of the SoC should be periodically aligned to guarantee correctness in the operations of the BESS.

Table 3 reports the KPIs calculated for each MILP-based model, together with the computational effort required for the simulation. The SoC MRE made it possible to highlight how the fast-piecewise method showed the best computational performance among those under all the three methods. Moreover, it coherently showed that the degree of accuracy increased with the computational effort.

5. Model testing: optimizing BESS scheduling in a real-life case study

The three developed models were validated, meaning their performances could be compared with that of a benchmark numerical model. A further testing procedure was useful in understanding how modeling performance could affect the results of an optimization process aimed at defining the operational schedule of a generic BESS. This was done by testing the MILP-based models on a real-life case study coinciding with a building of the Politecnico di Milano University campus located in the northern part of Milan. This building hosts classrooms and offices, having a high-power demand during the central part of the day (peak load of approximately 350 kW) and baseload consumption during the night (minimum load of 150 kW). The building load can be satisfied through a PV power plant connected under the same

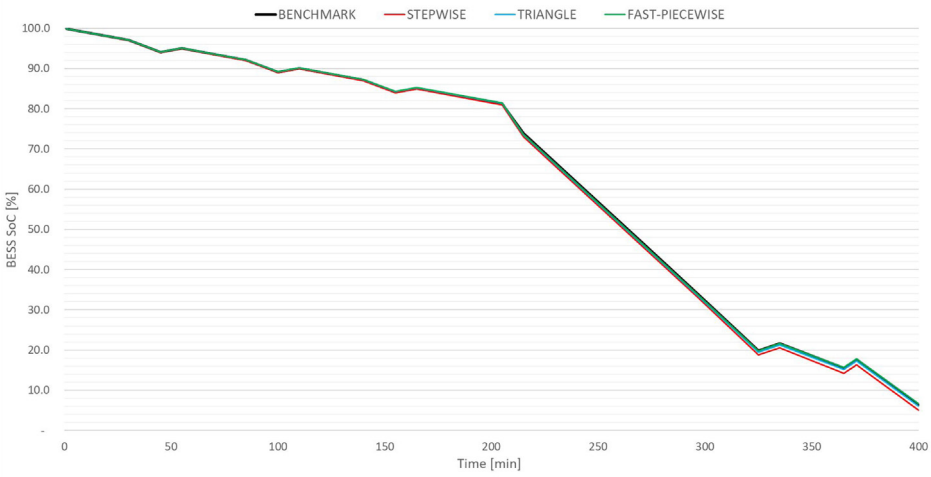

Fig. 9. Comparison between the evolution of the benchmark SoC during the simulation and the SoC values estimated by the three developed models.

Table 3
KPIs for MILP-based models.

MODEL	MAE_{SoC} [%]	$MAE_{efficiency}$ [%]	MRE_{SoC} [%]	Computational Effort [s]
Triangle	0.79	2.08	0.42	672
Stepwise	1.02	2.39	0.44	302
Fast-piecewise	0.91	2.46	0.51	10

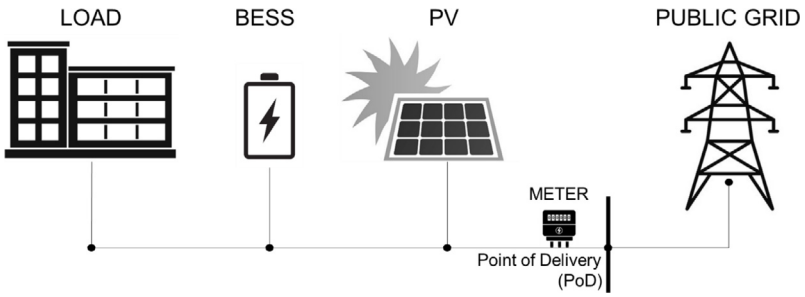

Fig. 10. Case study architecture considered for testing procedure.

low voltage (LV) substation; the PV plant has a nominal power of 800 kW, which is almost 230% of the peak load value; the case study is presented in Fig. 10. The testing procedure considered the power demand and data on the PV-produced power for three consecutive days.

Within the optimization problem, the BESS can charge and discharge whenever an optimal situation arises. The objective function involves the minimization of operating costs; the final variable considers the expenditure for the energy withdrawn from the public grid (ee^{bill}) and the revenues coming from selling energy. The energy sold (ee^{sold}) coincides with the energy injected into the public grid and is valued at the zonal market price (P^{zonal}). On the other hand, the electricity purchased (ee^{purch}) is paid according to a trinomial structure, with a fixed component (Ω^{POD}, in euro per point of connection); a power-based component (Ω^{kW}, in euro per kW of peak power withdrawn $ee^{with,MAX}$); and an energy-based component (the zonal price P^{zonal}, in euro per kWh of energy volume withdrawn). Finally, the electricity balance within the internal private grid includes the power produced by the PV plant (EE^{PV}); the electricity demand (EE^{LOAD}); the power charged ($ee^{BESS,charge}$) and discharged ($ee^{BESS,discharge}$) by the BESS; and, possibly, the energy injected or withdrawn from the public grid. The formulations for the objective function, electricity bill, and energy balance are reported in Eq. (5a), (5b) and (5c), respectively.

$$minimize\left(ee^{bill} - \sum_t \left(ee_t^{sold} * P_t^{zonal}\right)\right) \tag{5a}$$

$$e^{bill} = \sum_t \left(ee_t^{purch} * P_t^{zonal}\right) + \Omega^{kW} * ee^{with,MAX} + \Omega^{POD} \tag{5b}$$

$$\begin{aligned} ee_t^{in} &= ee_t^{out} \\ ee_t^{in} &= EE_t^{PV} + ee_t^{BESS,discharge} + ee_t^{purch} \\ ee_t^{out} &= EE_t^{LOAD} + ee_t^{BESS,charge} + ee_t^{sold} \end{aligned} \tag{5c}$$

Considering that the production of the PV plant cannot be controlled in a situation without the BESS, there will be some energy withdrawal during night-time and some injection during daytime (Fig. 11). The following sub-section compares the economic results of this reference situation (without any BESS) with a configuration obtained by adding a BESS rated 250 kW and 550 kWh; the BESS was alternatively scheduled by exploiting each of the three previously introduced MILP-based models.

While power injection has fully energy-based remuneration, energy withdrawal is valued in the electricity bill according to a mixed, capacity, and energy-based payment. In this context, a BESS is expected to provide the following:

- an arbitrage service, exploiting the different market prices during the time considered; and

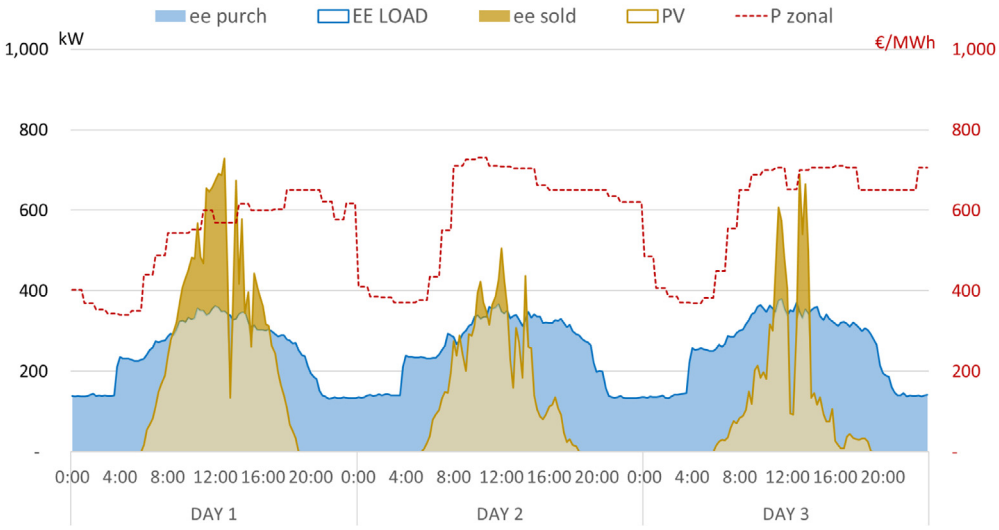

Fig. 11. Power exchanges during the three days of the testing procedure: reference configuration without any BESS.

Table 4
Technical and economic results of the testing procedure.

	u.m.	Ref. Case W/O BESS	With BESS Stepwise Model	With BESS Triangle Model	With BESS Fast-Piecewise Model
Technical Data					
Consumption	kWh	18,068	18,299	18,421	18,413
Production	kWh	9,474	9,474	9,474	9,474
Self-consumption	kWh	7,682	8,951	8,860	8,720
Withdrawal	kWh	10,385	9,347	9,560	9,693
Peak power withdrawn	kW	314	267	295	294
Injection	kWh	1,792	523	614	754
BESS-mean efficiency	%	–	89.70%	91.34%	91.74%
BESS-energy cycled	kWh	–	3,033	3,368	3,487
BESS-auxiliary demand	kWh	–	105	84	83
Economic Data					
Bill-power comp. (A)	€	1,580	1,340	1,485	1,476
Bill-energy comp. (B)	€	5,775	4,775	4,723	4,766
Bill-PoD comp. (C)	€	122	122	122	122
Bill–total (D=A+B+C)	€	10,244	8,628	8,763	8,845
Electricity sold (E)	€	1,112	315	371	476
Opex (D - E)	€	9,132	8,313	8,393	8,369

- a peak-shaving service, reducing the peaks in power withdrawal as much as possible.

5.1. Results of testing procedure

Optimized scheduling over a three-day horizon using a 15 min time-step was carried out by exploiting the three MILP-based BESS models; the technical and economic results are presented in Table 4.

Examining the technical performances shown in Table 4, the energy consumption increases with respect to the reference case (without the BESS), owing to the presence of an energy demand from the BESS auxiliaries and some energy losses during the charging and discharging cycles of the BESS. This higher energy demand varies from a maximum of +2% (fast-piecewise model) to a minimum of +1.2% (stepwise model), depending on the model.

Second, the BESS supports an increase in the self-consumption of PV generated power, with small differences between the different BESS modeling approaches, with the self-consumption being 15% greater than that in the reference case. Additionally, both the withdrawal and injection of energy were consequences of the self-consumption level. Indeed, greater self-consumption of energy implies that less energy has been withdrawn and injected.

Third, peak power withdrawal (calculated on a 15-minutes base) decreased owing to the BESS, confirming that the BESS had been exploited to provide a peak-shaving service, driven by the presence of a €/kW tariff on the peak capacity withdrawn. The peak power decreased by 20 kW under both the triangle and fast-piecewise models, with its decrease ranging between 40 and 50 kW under the stepwise model.

Differences considered from a technical standpoint also reflected the economic results. Particularly, while the impact of the BESS modeling approach on the overall operating expenditures (coinciding with the objective function) seemed modest, within a range of +/−1%, looking at the single cost components, certain differences could be observed. Indeed, the stepwise model underestimated the costs associated with peak power, with a −10% estimation with respect to that under the triangle model. On the other hand, differences in the energy cost estimation were

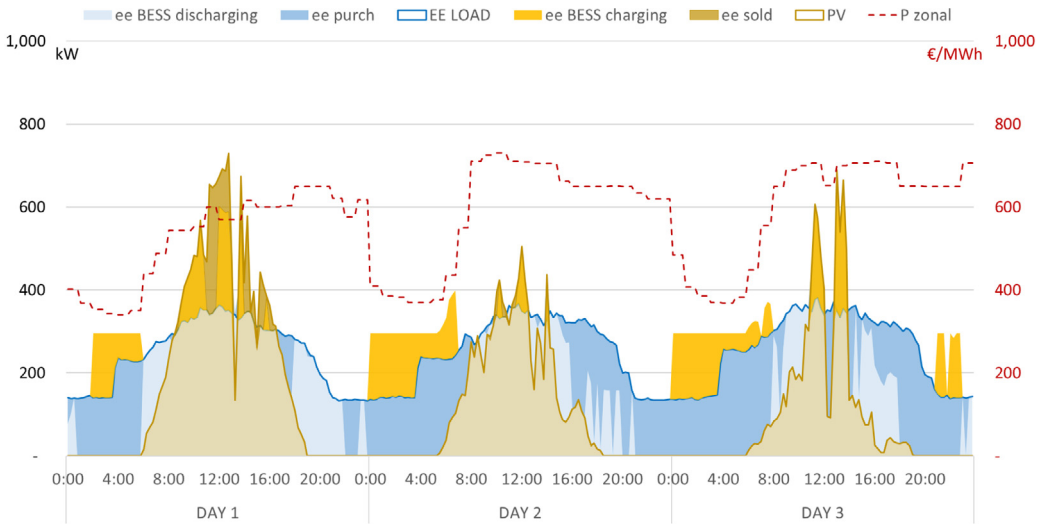

Fig. 12. Power exchanges during the three days of testing procedure. Configuration with an installed BESS and the exploitation of the *triangle* modeling approach.

smaller, while they remained when considering the estimated value of energy injection.

Finally, when looking at the BESS power profiles, the different services for which the BESS was exploited could be classified. Particularly, the following observations were obtained (Fig. 12).

- The BESS was charging both during the night-time, when prices (red dashed line) were low, and during the daytime, but only when there over-generation from the PV; the energy coming from the PV panels was stored in the BESS instead of being injected into the grid;
- The BESS was discharging during the morning and evening load ramps, which was exacerbated by the PV plant, due to which the power went from being withdrawn and injected into the grid and vice versa (from 6:00 to 10:00 and from 16:00 to 20:00).

Power was discharged during the net-load ramps to reduce the energy withdrawal during hours characterized by high prices (red dashed line). Indeed, the peak power withdrawal was increased during the night when prices were lower to exploit the energy stored during more expensive hours.

6. Conclusion

This study presents three novel mathematical approaches to model complex BESS performances that consider both storage parameters (SoC and C-rate) and external conditions (ambient temperature and auxiliary consumption). The presented models explored the trade-off between modeling accuracy and computational effort. Particularly, the fast-piecewise mathematical formulation resulted in a good compromise, providing a great computational performance and proper modeling accuracy. Finally, a testing procedure based on a real-life case study showed that the different BESS modeling approaches could significantly impact the optimization results, with different operational setpoints being imposed on the BESS schedule.

The development of new mathematical formulations to model the complexity of BESS performance is fundamental for scheduling them optimally, particularly with the growing need for near real-time optimization tools for multi-energy systems where BESS play a key role. This study presented three different MILP-based formulations, validating them against a benchmark numerical model exploiting an IEC 62660-1 based test cycle. Two out of the three models showed a fundamental imbalance between the computational time and modeling accuracy. However, the fast-piecewise formulation resulted in a good balance between the two, showing a great potential for application in near real-time problems requiring a high modeling accuracy. Finally, the study reported a test case wherein all the three models developed were tested on a real-life case study. The results showed that exploiting modeling tools with slightly different performances could greatly diversify the optimization results, which is fundamental for the on-field application of optimization tools, and hinder the requested rate of return for a BESS investment.

Table 5 summarizes the main advantages and drawbacks of the three modeling approaches introduced in the study. As reported in Table 3, the triangle formulation shows the highest accuracy, but suffers from a significant burden in terms of needed computational time. The stepwise formulation halves the computational time, but loses in precision. Finally, the fast-piecewise formulation has a computational time that is almost two orders of magnitude lower than the triangle one, while at the same time containing the accuracy loss, possibly overperforming the stepwise approach. In addition, the fast-piecewise formulation allows, when building the BESS performance map through an on-field testing campaign, to sample and characterize it even only in a partial manner, still keeping the modeling accuracy high; however, this is possible only if non-linearities in BESS performance are confined to specific operational regions: for performance maps strongly non-linear, the fast-piecewise approach should be excluded.

The obtained results allow to draw two main conclusions. First, it is possible to formulate and exploit specific approaches dedicated to BESS modeling that show a proper trade-off between accuracy and computational effort. The fast-piecewise method, thanks to its fast computation time, could fit with a Model Predictive Control (MPC) strategy for real-time BESS operations, coupling it with appropriate state-forecast simulation tools. This kind of application could be particularly relevant in the context of control architectures based on edge computing, where the optimal operation of the assets near real-time is left to on-field controllers rather than to cloud ones. Second, the exploitation of different modeling approaches for BESS performance simulation can result in very diverse operational setpoints, thus largely changing the economic profit coming from BESS operations. This aspect holds significant importance considering the growing emphasis on services and revenue stacking, which has emerged as a promising means of recouping BESS investments. When multiple services

Table 5
Comparison of the developed modeling approaches.

MODEL	Advantages	Disadvantages
Triangle	• High accuracy	• High computational time • Need to characterize the whole performance map
Stepwise	• Average computational time	• Low accuracy • Need to characterize the whole performance map
Fast-piecewise	• Very low computational time • Good accuracy (with smooth performance map) • Possibility to characterize the performance map only partially	• Limited application for highly non-linear performance maps

coincide across various time horizons, ranging from month-ahead to intra-day, employing an appropriate modeling approach can make a substantial difference as each scheduling step influences subsequent ones. Therefore, it is possible to employ a highly accurate modeling approach, such as the triangle model, for long and mid-term optimization scheduling, while leveraging the low latency of a lightweight modeling approach, like the fast-piecewise model, for short-term operations.

Three main considerations still remain. First, it is necessary to understand the resilience of each modeling approach with respect to the different types of electrochemical storage technologies. This analysis is expected to be affected by the non-linearities shown by each storage technology within its own performance map. Second, it is necessary to evaluate the impact of battery aging on BESS modeling; the contribution of both calendar and cycling aging on the variation of the BESS performance map in time should be quantitatively assessed. Third, for the real-time optimization of the BESS power set-point, it is necessary to develop a tool that can monitor the state-of-health and performance of the BESS and consequently update the LUT and optimization parameters of the BESS in a coherent manner.

CRediT authorship contribution statement

Filippo Bovera: Conceptualization, Methodology, Software, Validation, Resources, Visualization, Writing – original draft, Writing – review & editing. **Matteo Spiller:** Methodology, Software, Investigation, Formal analysis, Resources, Data curation. **Matteo Zatti:** Conceptualization, Methodology, Validation, Writing – review & editing. **Giuliano Rancilio:** Conceptualization, Resources, Data curation. **Marco Merlo:** Conceptualization, Writing – review & editing, Supervision.

Declaration of competing interest

The authors declare that they have no known competing financial interests or personal relationships that could have appeared to influence the work reported in this paper.

Data availability

Data will be made available on request.

Appendix A. Complete mathematical formulation of developed models

The complete mathematical formulation for all the three modeling approaches presented in the paper is reported below.

A.1. Triangle formulation

In the triangle formulation, BESS operating setpoint is defined through the following constraints, where t is the optimization period, i and j are the indexes of the charging and discharging LUTs.

[Bool] $$\sum_i \sum_j y_{i,j,t}^{cha} = z_t^{cha},\ 0 \le y_{j,t}^{cha} \le 1 \quad \forall t \quad (A.1a)$$

[Bool] $$\sum_i \sum_j y_{i,j,t}^{dis} = z_t^{dis},\ 0 \le y_{j,t}^{dis} \le 1 \quad \forall t \quad (A.1b)$$

[Bool] $$z_t^{cha} + z_t^{dis} \le 1 \quad \forall t \quad (A.1c)$$

[p.u.] $$p_t^{dis,DC} = \sum_i \sum_j P_{i,t}^{dis,DC} * y_{i,j,t}^{dis} \quad \forall t \quad (A.1d)$$

[p.u] $$p_t^{dis,AC} = \sum_i \sum_j P_{i,j,t}^{dis,AC} * y_{i,j,t}^{dis} \quad \forall t \quad (A.1e)$$

[p.u.] $$p_t^{cha,DC} = \sum_i \sum_j P_{i,j,t}^{cha,DC} * y_{i,j,t}^{cha} \quad \forall t \quad (A.1f)$$

[p.u.] $$p_t^{cha,AC} = \sum_i \sum_j P_{i,t}^{cha,AC} * y_{i,j,t}^{cha} \quad \forall t \quad (A.1g)$$

[%] $$soc_t = \sum_i \sum_j SOC_{j,t}^{dis} * y_{i,j,t}^{dis} + \sum_i \sum_j SOC_{j,t}^{cha} * y_{i,j,t}^{cha} \quad \forall t \quad (A.1h)$$

[kWh] $$E^{BESS,nom} * soc_t = e_t \quad \forall t \quad (A.1i)$$

[kWh] $$e_t^{BESS} = e_{t-1}^{BESS} + \left(p_t^{cha,DC} - p_t^{dis,DC}\right) * P^{BESS,nom} * \Delta t \quad \forall t \quad (A.1j)$$

[Bool] $$\sum_i \sum_j \left(h_{i,j,t}^{up\ cha} + h_{i,j,t}^{low\ cha}\right) = z_t^{cha} \quad \forall t \quad (A.1k)$$

[Bool] $$\sum_i \sum_j \left(h_{i,j,t}^{up\ dis} + h_{i,j,t}^{low\ dis}\right) = z_t^{dis} \quad \forall t \quad (A.1l)$$

[Bool] $$h_{i+1,j+1,t}^{up\ cha} + h_{i+1,j+1,t}^{low\ cha} + h_{i,j+1,t}^{low\ cha} + h_{i+1,j,t}^{up\ cha} + h_{i,j,t}^{up\ cha} + h_{i,j,t}^{low\ cha} \ge y_{i,j,t}^{cha} \quad \forall t \quad (A.1m)$$

[Bool] $$h_{i+1,j+1,t}^{up\ dis} + h_{i+1,j+1,t}^{low\ dis} + h_{i,j+1,t}^{low\ dis} + h_{i+1,j,t}^{up\ dis} + h_{i,j,t}^{up\ dis} + h_{i,j,t}^{low\ dis} \ge y_{i,j,t}^{dis} \quad \forall t \quad (A.1n)$$

[Bool] $$h_{0,j,t}^{up\ cha} = h_{0,j,t}^{low\ cha} = h_{i,0,t}^{up\ cha} = h_{i,0,t}^{low\ cha} = 0 \quad \forall t \quad (A.1o)$$

[Bool] $$h_{0,j,t}^{up\ dis} = h_{0,j,t}^{low\ dis} = h_{i,0,t}^{up\ dis} = h_{i,0,t}^{low\ dis} = 0 \quad \forall t \quad (A.1p)$$

[Bool] $$h_{6,j,t}^{up\ cha} = h_{6,j,t}^{low\ cha} = h_{i,10,t}^{up\ cha} = h_{i,10,t}^{low\ cha} = 0 \quad \forall t \quad (A.1q)$$

[Bool] $$h_{6,j,t}^{up\ dis} = h_{6,j,t}^{low\ dis} = h_{i,10,t}^{up\ dis} = h_{i,10,t}^{low\ dis} = 0 \quad \forall t \quad (A.1r)$$

Equations (A.1a), (A.1b) and (A.1c) distinguish charging and discharging operations, where $y^{dis}_{i,j,t}$ and $y^{cha}_{i,j,t}$ are continuous variables ranging from 0 to 1, used to perform the convex hull of the sampling points $[i, j]$ in a given time instant. Their summation over all the points within the LUT should be equal to 1 or 0, depending on whether the BESS is charging or discharging, accordingly. Finally, z^{cha}_t and z^{dis}_t are binary variables regulating the charging/discharging dichotomy. Equations from (A.1d) to (A.1h) define the linear interpolation between the sampling points: based on the values assumed by $y^{dis}_{i,j,t}$ and $y^{cha}_{i,j,t}$, a specific weight is assigned to the LUT values (DC power, AC power and SoC, either in the discharging or charging phase). Hence, the corresponding variables ($p^{dis,DC}_t$, $p^{dis,AC}_t$, $p^{cha,DC}_t$, $p^{cha,DC}_t$, soc_t) are calculated as the weighted sum of the LUT values, where weights are provided by $y^{dis}_{i,j,t}$ and $y^{cha}_{i,j,t}$. Eq. (A.1i) links the SoC value to the energy content of the storage, updated in every time interval according to the power exchanged by the BESS and Eq. (A.1j) enforces the energy storage level according to the power exchanged by the BESS. Eqs. (A.1k) and (A.1l) introduce the triangle binary variables $\left(h^{up\ cha}_{i,j,t}, h^{low\ cha}_{i,j,t}\right)$ and $\left(h^{up\ dis}_{i,j,t}, h^{low\ dis}_{i,j,t}\right)$: they represent the upper and lower triangles defined for each 4-tuple of adjacent sampling points. Thanks to such two equations, the triangle binary variables are equal to one when the specific triangle is activated, zero otherwise. Eqs. (A.1m) and (A.1n) limits the $y^{dis}_{i,j,t}$ and $y^{cha}_{i,j,t}$ variables to be different from zero only when the corresponding triangle is selected thanks to the previous three equation. This way, the convex hull is computed among the vertexes of the specific triangle that contains the current BESS setpoint. The last four Equations (from (A.1o) to (A.1r)) are there to force the deactivation of the boundary triangles, which are all those triangles actually laying outside of the performance map (hence making no sense, physically speaking), but still needed to keep the mathematical formulation consistent.

A.2. Stepwise formulation

In the stepwise formulation, BESS operating setpoint is defined through the following constraints, where, t is the calculation period, i, j and k are the indexes of charging, discharging and idle LUTs.

[Bool] $$\sum_i \sum_j x^{dis}_{i,j,t} = z^{dis}_t,\ x^{dis}_{i,j,t} \in [0,\ 1] \quad \forall t \tag{A.2a}$$

[Bool] $$\sum_i \sum_j x^{cha}_{i,j,t} = z^{cha}_t,\ x^{cha}_{i,j,t} \in [0,\ 1] \quad \forall t \tag{A.2b}$$

[Bool] $$z^{dis}_t + z^{cha}_t \le 1 \quad \forall t \tag{A.2c}$$

[p.u.] $$x^{cha}_{i,j,t} * P^{cha,AC}_{i,t} \le p^{cha,AC}_{i,j,t} \le x^{cha}_{i,j,t} * P^{cha,AC}_{i+1,t} \quad \forall t \tag{A.2d}$$

[p.u.] $$x_{i,j,t} * P^{dis,DC}_{i,t} \le p^{dis,DC}_{i,j,t} \le x_{i,j,t} * P^{dis,DC}_{i+1,t} \quad \forall t \tag{A.2e}$$

[p.u.] $$p^{dis,AC}_t = \sum_i \sum_j p^{dis,DC}_{i,j,t} * \eta^{dis}_{i,j} \quad \forall t \tag{A.2f}$$

[p.u.] $$p^{cha,DC}_t = \sum_i \sum_j p^{cha,AC}_{i,j,t} * \eta^{cha}_{i,j} \quad \forall t \tag{A.2g}$$

[%] $$x^{cha}_{i,j,t} * SOC^{cha}_{j,t} \le soc^{cha}_{i,j,t} \le x^{cha}_{i,j,t} * SOC^{cha}_{j+1,t} \quad \forall t \tag{A.2h}$$

[%] $$x^{dis}_{i,j,t} * SOC^{dis}_{j,t} \le soc^{dis}_{i,j,t} \le x_{i,j,t} * SOC^{dis}_{j+1,t} \quad \forall t \tag{A.2i}$$

[%] $$soc_t = \sum_i \sum_j \left(soc^{cha}_{i,j,t} + soc^{dis}_{i,j,t}\right) \quad \forall t \tag{A.2j}$$

[kWh] $$e^{BESS}_t = E^{BESS,nom} * \mathrm{soc_t} \quad \forall t \tag{A.2k}$$

[kWh] $$e^{BESS}_t = e^{BESS}_{t-1} + \left(p^{cha,DC}_t - p^{dis,DC}_t\right) * P^{BESS,nom} * \Delta t \quad \forall t \tag{A.2l}$$

Equations (A.2a), (A.2b) and (A.2c) distinguish charging and discharging operations, where $x^{cha}_{i,j,t}$ and $x^{dis}_{i,j,t}$ are binary variables used to activate a specific power-SoC interval $[i, j]$ (a "step") in a given time instant t. As a consequence, z^{cha}_t and z^{dis}_t, also binary variables, regulate the charging/discharging dichotomy. Eqs. (A.2d) and (A.2e) identify the powers intervals to be activated in the given time period for both the charging and the discharging phases; the same formulation is exploited for the SoC in Eqs. (A.2h) and (A.2i). Eqs. (A.2f) and (A.2g) allow to calculate the AC-side discharging or DC-side charging power corresponding to the selected operating interval through the application of the discharging or charging efficiency (parameters derived from the corresponding LUT). Finally, Eqs. (A.2j) and (A.2k) correlate the LUT identification of the SoC with the current value of energy stored in the BESS, expressed in kWh. Eq. (A.2l) updates the energy storage level according to the power exchanged by the BESS, ensuring the coherence between SoC update and power exchanged.

A.3. Fast-piecewise formulation

In the fast-piecewise formulation, BESS operating setpoint is defined through the following constraints, where, t is the calculation period, i, j and k are the indexes of charging, discharging and idle LUTs.

[Bool] $$\sum_j y^{dis}_{j,t} = z^{dis}_t,\ 0 \le y^{dis}_{j,t} \le 1 \quad \forall t \tag{A.3a}$$

[Bool] $$\sum_i y^{cha}_{i,t} = z^{cha}_t,\ 0 \le y^{cha}_{j,t} \le 1 \quad \forall t \tag{A.3b}$$

[Bool] $$\sum_k y^{idle}_{k,t} = z^{idle}_t,\ 0 \le y^{idle}_{k,t} \le 1 \quad \forall t \tag{A.3c}$$

[Bool] $$z^{dis}_t + z^{cha}_t + z^{idle}_t \le 1 \quad \forall t \tag{A.3d}$$

[p.u.] $$p^{dis,DC}_t = \sum_j P^{dis,DC}_{j,t} * y^{dis}_{j,t} \quad \forall ft \tag{A.3e}$$

[p.u.] $$p^{dis,AC}_t = \sum_j P^{dis,AC}_{j,t} * y^{dis}_{j,t} \quad \forall t \tag{A.3f}$$

[p.u.] $$p^{cha,DC}_t = \sum_i P^{cha,DC}_{i,t} * y^{cha}_{i,t} \quad \forall t \tag{A.3g}$$

[p.u.] $$p^{cha,AC}_t = \sum_i P^{cha,AC}_{i,t} * y^{cha}_{i,t} \quad \forall t \tag{A.3h}$$

[p.u.] $$soc_t = \sum_j SOC^{dis}_{j,t} * y^{dis}_{j,t} + \sum_i SOC^{cha}_{i,t} * y^{cha}_{i,j,t} + \sum_k SOC^{idle}_{k,t} * y^{idle}_{k,t} \quad \forall t \tag{A.3i}$$

[kWh] $$e^{BESS}_t = e^{BESS}_{t-1} + \left(p^{cha,DC}_t - p^{dis,DC}_t\right) * P^{BESS,nom} * \Delta t \quad \forall t \tag{A.3j}$$

[kWh] $$E^{BESS,nom} * soc_t = e_t \quad \forall t \tag{A.3k}$$

Table B.1
Look-up table (LUT) used to linearize the capability limits imposed by the BMS.

Index	SoC	$P^{CC,dis}$ [p.u.]	$P^{CC,cha}$ [p.u.]
1	0%	1.00	0.09
2	2%	1.00	0.72
3	5%	1.00	1.00
4	95%	0.54	1.00
5	100%		

Equations (A.3a), (A.3b), (A.3c) and (A.3d) distinguish charging, discharging and idle operations, where $y_{j,t}^{dis}$, $y_{i,t}^{cha}$ and $y_{k,t}^{idle}$ are continuous variables ranging from 0 to 1, used to perform the linear interpolation between LUT's sampling points in a given time instant. Their summation over all the points within the LUT should be equal to 1 or 0, depending on whether the BESS is charging, discharging or idle, accordingly. Finally, z_t^{cha}, z_t^{dis} and z_t^{idle} are binary variables regulating the charging, discharging or idle operations trichotomy. Equations from (A.3e), (A.3i) define the linear interpolation between the sampling points: based on the values assumed by where $y_{j,t}^{dis}$, $y_{i,t}^{cha}$ and $y_{k,t}^{idle}$, a specific weight is assigned to the LUT values (DC power, AC power and SoC, either in the discharging or charging phase, only SoC in the idle phase). Hence, the corresponding variables ($p_t^{dis,DC}$, $p_t^{dis,AC}$, $p_t^{cha,DC}$, $p_t^{cha,DC}$, soc_t) are calculated as the weighted sum of the LUT values, where weights are provided by $y_{j,t}^{dis}$, $y_{i,t}^{cha}$ and $y_{k,t}^{idle}$. Eq. (A.3j) links the SoC value to the energy content of the storage, updated in every time interval according to the power exchanged by the BESS and Eq. (A.3k) enforces the energy storage level according to the power exchanged by the BESS.

Appendix B. Mathematical formulation for BMS capability limits and auxiliary systems

Two further modeling blocks are included in the problem formulation, emulating the capability limits imposed by the BMS and the energy demand for auxiliaries. First, capability limits are modeled linearizing the two curves presented in Fig. 2(b) for the discharging and charging phases. This is done exploiting a LUT where the SoC is correlated with the maximum available discharging and charging power. In particular, the LUT used to linearize the capability curve is reported in Table B.1.

The mathematical formulation to linearize the capability curve limits is reported below. Two variables ranging from zero to one are used to weight the LUT sampling points, namely $y_{j,t}^{CC,dis}$ and $y_{j,t}^{CC,cha}$. Eqs. (B.1a) and (B.1b) impose their summation along LUT's index to be equal to one. Depending on BESS SoC (soc_t), Equations from (B.1c) to (B.1f) regulate the values of $y_{j,t}^{CC,dis}$ and $y_{j,t}^{CC,cha}$ in order to select the correct LUT interval. Based on these values, maximum discharging and charging powers ($p_t^{MAX,dis}$ and $p_t^{MAX,cha}$) are computed through the linear interpolation between power limits imposed by the capability curves at the specific SoC value ($P_{j,t}^{CC,dis}$ and $P_{j,t}^{CC,cha}$) (Eqs. (B.1g) and (B.1h)). Finally, BESS power set-point, being the AC-side discharging or charging power ($p_t^{dis,AC}$ and $p_t^{cha,AC}$), is limited to be lower than the maximum power imposed by capability curve limits through Eqs. (B.1i) and (B.1j).

$$[\text{Bool}] \quad \sum_k y_{k,t}^{CC,dis} = 1,\ 0 \le y_{k,t}^{CC,dis} \le 1 \quad \forall t \quad \text{(B.1a)}$$

$$[\text{Bool}] \quad \sum_k y_{k,t}^{CC,cha} = 1,\ 0 \le y_{k,t}^{CC,cha} \le 1 \quad \forall t \quad \text{(B.1b)}$$

$$[\%] \quad soc_t \ge \sum_k \overline{SOC_{k,t}^{CC}} * y_{k,t}^{CC,dis} \quad \forall t \quad \text{(B.1c)}$$

$$[\%] \quad soc_t \le \sum_k \overline{SOC_{k+1,t}^{CC}} * y_{k,t}^{CC,dis} \quad \forall t \quad \text{(B.1d)}$$

Table B.2
Look-up table (LUT) used for auxiliaries' consumption.

Index	T^{amb} [°C]	P^{AC} [p.u.]	P^{AUX} [p.u.]
1	0	0.00	0.00288
2	40	0.00	0.00554
3	0	1.00	0.00633
4	40	1.00	0.01141

Table C.1
Generic LUT for fast-piecewise interpolation.

Index	PAC [p.u.]	PDC [p.u.]	η BESS
1	0.450	0.500	90%
2	0.002	0.010	20%
3	0	0	ND

$$[\%] \quad soc_t \ge \sum_k \overline{SOC_{k,t}^{CC}} * y_{k,t}^{CC,cha} \quad \forall t \quad \text{(B.1e)}$$

$$[\%] \quad soc_t \le \sum_k \overline{SOC_{k+1,t}^{CC}} * y_{k,t}^{CC,cha} \quad \forall t \quad \text{(B.1f)}$$

$$[\text{p.u.}] \quad p_t^{MAX,dis} = \sum_k \overline{P_{k,t}^{CC,dis}} * y_{k,t}^{CC,dis} \quad \forall t \quad \text{(B.1g)}$$

$$[\text{p.u.}] \quad p_t^{MAX,cha} = \sum_k \overline{P_{k,t}^{CC,cha}} * y_{k,t}^{CC,cha} \quad \forall t \quad \text{(B.1h)}$$

$$[\text{p.u.}] \quad p_t^{dis,AC} \le p_t^{MAX,dis} \quad \forall t \quad \text{(B.1i)}$$

$$[\text{p.u.}] \quad p_t^{cha,AC} \le p_t^{MAX,cha} \quad \forall t \quad \text{(B.1j)}$$

Second, auxiliaries are modeled through a set of linear constraints. The LUT reported in Table B.2 is used to calculate auxiliaries consumption depending on ambient temperature and on AC-side requested power; all powers are expressed in per unit as a function of BESS nominal capacity.

The mathematical formulation used to compute auxiliaries' demand through the LUT reported above is presented in equations below. A variable ranging from zero to one ($y_{k,t}^{AUX}$) is used weight the points of auxiliaries LUT (Eq. (B.2a)). Its value is chosen based on the ambient temperature (T_t^{AMB}, given as an input) in Eq. (B.2b), and on BESS AC-side power in Eq. (B.2c), calculated through one of the three approaches presented above. Finally, depending on $y_{k,t}^{AUX}$ value, auxiliaries setpoint is computed in Eq. (B.2d), expressed in per unit.

$$[\text{Bool}] \quad \sum_k y_{k,t}^{AUX} = 1,\ 0 \le y_{k,t}^{AUX} \le 1 \quad \forall t \quad \text{(B.2a)}$$

$$[°\text{C}] \quad T_t^{AMB} = \sum_k y_{k,t}^{AUX} * T_{k,t}^{AUX} \quad \forall t \quad \text{(B.2b)}$$

$$[\text{p.u.}] \quad p_t^{dis,AC} + p_t^{cha,AC} = \sum_k y_{k,t}^{AUX} * P_{k,t}^{AC} \quad \forall t \quad \text{(B.2c)}$$

$$[\text{p.u.}] \quad p_t^{AUX} = \sum_k y_{k,t}^{AUX} * P_{k,t}^{AUX} \quad \forall t \quad \text{(B.2d)}$$

Appendix C. Nonlinearity demonstration for zero-power set-point in the fast-piecewise formulation

Let us consider a generic LUT presenting AC-side and DC-side power sampling points. It is possible to associate some efficiencies to each of the sampling points (see Table C.1).

If the optimization procedure requires to have an AC-side power of 0.01 [p.u.] and the LUT includes also zero-power sampling points, the discharging efficiency will be far from being the real, expected one. Indeed:

CASE (1): NO ZERO-POWER POINTS

$$p^{dis,AC} = 0.01\,[p.u.] = x_1 * P_1^{dis,AC} + x_2 * P_2^{dis,AC}$$
$$= 0.01785 * 0.45 + 0.98215 * 0.002$$
$$p^{dis,DC} = 0.01785 * 0.5 + 0.98215 * 0.01 = 0.01875\ [\text{p.u.}]$$
$$\eta_{BESS} = \frac{p^{dis,AC}}{p^{dis,DC}} = 53.33\%$$

CASE (2): WITH ZERO-POWER POINTS

$$p^{dis,AC} = 0.01\,[p.u.] = x_1 * P_1^{dis,AC} + x_3 * P_3^{dis,AC}$$
$$= 0.02222 * 0.45 + 0.97778 * 0$$
$$p^{dis,DC} = 0.02222 * 0.5 + 0.97778 * 0 = 0.01111\ [\text{p.u.}]$$
$$\eta_{BESS} = \frac{p^{dis,AC}}{p^{dis,DC}} = 90.00\%$$

which shows that zero-power points allow to artificially maintain the discharging efficiency at very high values. Since this high efficiency condition is favorable for BESS operations, then this trick will be systematically adopted during the optimization procedure, thus cheating on real performances and decreasing the modeling accuracy.

References

[1] IEA, Global Energy Review, IEA, Paris, 2021.
[2] M. Ding, W. Wang, X. Wang, Y. Song, D. Chen, M. Sun, A review on the effect of large-scale PV generation on power systems, Proc. Chinese Soc. Electr. Eng. 34 (1) (2014) 1–14.
[3] G. Delille, B. Francois, G. Malarange, Dynamic frequency control support by energy storage to reduce the impact of wind and solar generation on isolated power system's inertia, IEEE Trans. Sustain. Energy 3 (4) (2012) 931–939.
[4] E. Lannoye, D. Flynn, M. O'Malley, Evaluation of power system flexibility, IEEE Trans. Power Syst. 27 (2) (2012) 922–931.
[5] P. Denholm, M. Hand, Grid flexibility and storage required to achieve very high penetration of variable renewable electricity, Energy Policy 39 (3) (2011) 1817–1830.
[6] M. Alizadeh, M. Parsa Moghaddam, N. Amjady, P. Siano, M. Sheikh-El-Eslami, Flexibility in future power systems with high renewable penetration: A review, Renew. Sustain. Energy Rev. 57 (2016) 1186–1193.
[7] W. Cole, W.A. Frazier, A. Chad, Cost Projections for Utility-Scale Battery Storage: 2021 Update, National Renewable Energy Laboratory, Golden CO, 2021.
[8] IRENA, Electricity Storage and Renewables: Costs and Markets to 2030, International Renewable Energy Agency, Abu Dhabi, 2017.
[9] IEA, Grid-Scale Storage, International Energy Agency, Paris, 2021.
[10] S. Englberger, A. Jossen, H. Hesse, Unlocking the potential of battery storage with the dynamic stacking of multiple applications, Cell Rep. Phys. Sci. 1 (11) (2020).
[11] P.V. Brogan, R. Best, J. Morrow, R. Duncan, M. Kubik, Stacking battery energy storage revenues with enhanced service provision, IET Smart Grid 3 (4) (2020).
[12] G. Rancilio, F. Bovera, M. Merlo, Revenue stacking for BESS: Fast frequency regulation and balancing market participation in Italy, Int. Trans. Electr. Energy Syst. 2022 (2022).
[13] A. Baldinelli, A. Staffolani, G. Bidini, L. Barelli, F. Nobili, An extensive model for renewable energy electrochemical storage with Solid Oxide Cells based on a comprehensive analysis of impedance deconvolution, J. Energy Storage 33 (2022).
[14] S. Barcellona, A novel lithium ion battery model: A step towards the electrochemical storage systems unification, in: 2017 6th International Conference on Clean Electrical Power: Renewable Energy Resources Impact, ICCEP 2017, Santa Margherita Ligure, 2017.
[15] R. Attias, M. Salama, R. Pant, Y. Gofer, D. Aubarch, Modulation, characterization, and engineering of advanced materials for electrochemical energy storage applications: MoO3/V2O5 bilayer model system, J. Phys. Chem. C 123 (27) (2019) 16577–16587.
[16] Z. Li, P.-J. Qin, J.-Z. Chen, Y.-B. Che, Y.-B. Cai, Parameter detection model and simulation of energy storage lithium battery considering thermal characteristics, in: 2019 16th International Computer Conference on Wavelet Active Media Technology and Information Processing, ICCWAMTIP 2019, Chengdu, Sichuan Province, 2019.
[17] A. Urtasun, P. Sanchis, F. Guinjoan, L. Marroyo, Parameter-independent battery control based on series and parallel impedance emulation, IEEE Access 7 (2019) 70021–70031.
[18] A. Urtasun, A. Berrueta, P. Sanchis, L. Marroyo, Parameter-independent control for battery chargers based on virtual impedance emulation, IEEE Trans. Power Electron. 33 (10) (2018) 8848–8858.
[19] D. Karnopp, Bond graph models for electrochemical energy storage : Electrical, chemical and thermal effects, J. Franklin Inst. 327 (6) (1990) 983–992.
[20] J.R. Miller, S. Butler, Storage system design based on equivalent-circuit-model simulations: Comparison of eight different electrochemical capacitor storage systems, J. Power Sources 491 (2021).
[21] R. Drummond, G. Valmorbida, S.R. Duncan, Equivalent circuits for electrochemical supercapacitor models, IFAC-PapersOnLine 50 (1) (2017) 2671–2676.
[22] G. Nobile, Cacciato M., G. Scarcella, G. Scelba, Performance assessment of equivalent-circuit models for electrochemical energy storage systems, in: Proceedings IECON 2017 - 43rd Annual Conference of the IEEE Industrial Electronics Society, Beijing, 2017.
[23] G. Rancilio, A. Lucas, E. Kotsakis, G. Fulli, M. Merlo, M. Delfanti, M. Masera, Modeling a large-scale battery energy storage system for power grid application analysis, Energies (2019).
[24] A.J. Gonzalez-Castellanos, D. Ponzo, A. Bischi, Non-ideal linear operation model for li-ion batteries, IEEE Trans. Power Syst. 35 (1) (2019) 672–682.
[25] B. Pickering, S. Ikeda, R. Choudhary, R. Ooka, Comparison of metaheuristic and linear programming models for the purpose of optimising building energy supply operation schedule, in: Proceedings of the 12th REHVA World Congress, Aalborg, 2016.
[26] R. Dufo-Lopez, J. Bernal-Augustin, J. Contreras, Optimization of control strategies for stand-alone renewable energy systems with hydrogen storage, Renew. Energy 32 (7) (2007) 1102–1126.
[27] Y. Levron, J. Guerrero, Y. Beck, Optimal power flow in microgrids with energy storage, IEEE Trans. Power Syst. 28 (3) (2013) 3226–3234.
[28] G. He, Q. Chen, C. Kang, P. Pinson, Q. Xia, Optimal bidding strategy of battery storage in power markets considering performance-based regulation and battery cycle life, IEEE Trans. Smart Grid 7 (5) (2016) 2359–2367.
[29] A. Hawkes, M. Leach, Modelling high level system design and unit commitment for a microgrid, Appl. Energy 86 (7–8) (2009) 1253–1265.
[30] P. Harsha, M. Dahleh, Optimal management and sizing of energy storage under dynamic pricing for the efficient integration of renewable energy, IEEE Trans. Power Syst. 30 (3) (2015) 1164–1181.
[31] M. Marzband, M. Ghadimi, A. Sumper, J.L. Dominguez-Garcia, Experimental validation of a real-time energy management system using multi-period gravitational search algorithm for microgrids in islanded mode, Appl. Energy 128 (2014) 164–174.
[32] A. Malheiro, P. Castro, R.M. Lima, A. Estanqueiro, Integrated sizing and scheduling of wind/PV/diesel/battery isolated systems, Renew. Energy 83 (2015) 646–657.
[33] A. Ashouri, S.S. Fux, M.J. Benz, L. Guzzella, Optimal design and operation of building services using mixed-integer linear programming techniques, Energy 59 (2013) 365–376.
[34] M. Ippolito, M. Di Silvestre, R.S.E.G. Zizzo, G. Graditi, Multi-objective optimized management of electrical energy storage systems in an islanded network with renewable energy sources under different design scenarios, Energy 64 (2014) 648–662.
[35] R. Khalilpour, A. Vassallo, Planning and operation scheduling of PV-battery systems: A novel methodology, Renew. Sustain. Energy Rev. 53 (2016) 194–208.
[36] R. Mallol-Poyato, S. Salcedo-Sanz, S. Jimenez-Fernandez, P. Diaz-Villar, Optimal discharge scheduling of energy storage systems in MicroGrids based on hyper-heuristics, Renew. Energy 83 (2015) 13–24.
[37] G. Rancilio, M. Merlo, A. Lucas, Kostakis, M. Delfanti, Bess modeling: investigating the role of auxiliary system consumption in efficiency derating, in: International Symposium on Power Electronics, Electrical Drives, Automation and Motion, SPEEDAM, 2020.
[38] A. Sakti, K. Gallagher, N. Sepulveda, C. Uckun, C. Vergara, F. de Sisternes, D. Dees, A. Botterud, Enhanced representations of lithium-ion batteries in power systems models and their effect on the valuation of energy arbitrage applications, J. Power Sources 342 (2017) 279–291.
[39] Y.-G. Park, C.-W. Kim, J.-B. Park, MILP-based dynamic efficiency scheduling model of battery energy storage systems, J. Electr. Eng. Technol. 11 (5) (2016) 1063–1069.
[40] H. Pandzic, V. Bobanac, An accurate charging model of battery energy storage, IEEE Trans. Power Syst. 34 (2) (2019) 1416–1426.
[41] A. Grimaldi, F.D. Minuto, A. Perol, S. Casagrande, A. Lanzini, Ageing and energy performance analysis of a utility-scale lithium-ion battery for power grid applications through a data-driven empirical modelling approach, J. Energy Storage 65 (107232) (2023) 107232.